Theory of attosecond delays in molecular photoionization

Denitsa Baykusheva and Hans Jakob Wörner

Citation: The Journal of Chemical Physics **146**, 124306 (2017); doi: 10.1063/1.4977933
View online: http://dx.doi.org/10.1063/1.4977933
View Table of Contents: http://aip.scitation.org/toc/jcp/146/12
Published by the American Institute of Physics

Theory of attosecond delays in molecular photoionization

Denitsa Baykusheva and Hans Jakob Wörner[a)]
Laboratorium für Physikalische Chemie, ETH Zürich, Vladimir-Prelog-Weg 2, 8093 Zürich, Switzerland

(Received 1 November 2016; accepted 10 February 2017; published online 22 March 2017)

We present a theoretical formalism for the calculation of attosecond delays in molecular photoionization. It is shown how delays relevant to one-photon-ionization, also known as Eisenbud-Wigner-Smith delays, can be obtained from the complex dipole matrix elements provided by molecular quantum scattering theory. These results are used to derive formulae for the delays measured by two-photon attosecond interferometry based on an attosecond pulse train and a dressing femtosecond infrared pulse. These effective delays are first expressed in the molecular frame where maximal information about the molecular photoionization dynamics is available. The effects of averaging over the emission direction of the electron and the molecular orientation are introduced analytically. We illustrate this general formalism for the case of two polyatomic molecules. N_2O serves as an example of a polar linear molecule characterized by complex photoionization dynamics resulting from the presence of molecular shape resonances. H_2O illustrates the case of a non-linear molecule with comparably simple photoionization dynamics resulting from a flat continuum. Our theory establishes the foundation for interpreting measurements of the photoionization dynamics of all molecules by attosecond metrology. *Published by AIP Publishing.* [http://dx.doi.org/10.1063/1.4977933]

I. INTRODUCTION

In recent years, the techniques of attosecond spectroscopy have led to the observation and control of electron dynamics in atoms, molecules, and solids. One important branch of attosecond spectroscopy was initiated by the study of the real-time dynamics of photoionization, starting with photoemission from solids[1–3] and single-photon ionization of atoms.[4,5] These measurements have explored the natural attosecond time scale on which photoelectrons leave the parent species[6–9] with a recent emphasis on the role of atomic resonances.[10,11] In the case of atoms, the accepted interpretation of these measurements relies on the Eisenbud-Wigner-Smith time delay that can be defined for most scattering processes and more or less universal delays caused by the measurement.[12–15] Photoemission from solids is a much more complicated process in which the atomic contributions to the delay should also be important.[2,16,17] The field of photoemission delays has been comprehensively reviewed in Ref. 18.

Attosecond photoionization delays from molecules have received surprisingly little attention so far, presumably because of the associated experimental and theoretical complexity. Very recently, we have reported measurements of photoionization delays of N_2O and H_2O molecules[19,20] together with a brief summary of a theory that is fully outlined and developed in this article. Previously reported theoretical approaches to time-resolved molecular photoionization comprise calculations based on the solution of the full time-dependent Schrödinger equation for relatively simple prototypical systems such as H_2^+,[21–26] or restricted one-dimensional single-active-electron models of diatomic molecules.[27,28] Delays in one-photon ionization of N_2 and CO calculated using a Schwinger variational procedure were reported in Ref. 29. Here, we show that there is no simple additive relation between one-photon-ionization delays of molecules and those measured by attosecond interferometry. This difference between atoms and molecules arises from the facts that (i) molecules lack spherical symmetry such that multiple partial waves are required in the description of the initial bound state and (ii) the photoionization matrix elements depend on the orientation of the molecule relative to the ionizing radiation, such that delays measured in partially to randomly aligned molecules differ from those measured in the molecular frame in a non-trivial manner. Despite its inherent complexity, the understanding of molecular photoionization delays will however offer an attractive bridge between the complex world of the condensed phase and the transparent case of atoms. It also constitutes an essential step in extending attosecond metrology to molecular forms of matter, comprising clusters, liquids, and solids.

We now discuss the novelty of the information that can be obtained from attosecond time-resolved measurements of photoionization delays, as compared to more traditional variants of photoelectron spectroscopy. A complete description of photoionization within the dipole approximation requires the knowledge of the amplitude and phase of the transition dipole matrix elements from the bound initial state to the final continuum states. Photoelectron spectroscopy is frequently used to measure energy- and final-state resolved partial cross sections. These cross sections can be expressed as a sum of squared magnitudes of partial-wave matrix elements. Therefore, they are not sensitive to the phase of these matrix elements. Photoelectron angular distributions, in contrast, are defined by interference between different partial waves and are therefore

a)Electronic mail: woerner@phys.chem.ethz.ch. URL: http://www.atto.ethz.ch.

very sensitive to the phase shifts between degenerate continua.[30] However, frequency-domain measurements can only determine phase differences between photoelectron continua belonging to the same ionization threshold. Phase relations between ionization continua corresponding to different ionization thresholds cannot, in principle, be measured because the corresponding photoelectrons have a different kinetic energy. The techniques of time-domain spectroscopy do enable such measurements, provided that the bandwidth covered by the ionizing radiation exceeds the energetic separation of the considered ionization thresholds. Measurements of photoionization delays in molecules do therefore provide qualitatively new information on the dynamics of photoionization which is not accessible to frequency-domain methods. For this reason, comparisons of such measurements with theory are particularly interesting because they test a previously unexplored aspect of scattering calculations.

This article is structured as follows. Section II defines time delays in molecular photoionization. Starting from the (Eisenbud-Wigner-Smith) delays associated with single-photon ionization, defined in the molecular frame, we show how the delays measured by attosecond interferometry are obtained, first in the molecular frame and then in the laboratory frame. Section III illustrates these results for the case of two recently experimentally investigated molecules N_2O and H_2O[20] which illustrate the complementary cases of linear and non-linear molecules and additionally reveal the role of shape resonances on molecular photoionization delays. Section IV contains the conclusions of this article.

II. TIME DELAYS IN MOLECULAR PHOTOIONIZATION

The concept of time delay was introduced by Wigner[31] and Eisenbud[32] from a time-dependent perspective in the context of the scattering of wavepackets composed of spherical waves. By defining the concept of a "dwell time," Smith[33] arrived at an expression connecting the time delay with the properties of stationary eigenstates, in particular the S-matrix. While these concepts were restricted initially to the special case of short-range potential scattering, the concept of time-delay was shown after appropriate modifications to be transferable to systems subject to Coulomb interaction,[34,35] a situation relevant for the case of photoionization. In Sec. II A, we apply this concept to the case of molecular photoionization and outline the calculation of molecular time delays from state-of-the-art molecular quantum scattering theory currently employed in the theories of photoionization and photoelectron spectroscopies. The treatment of molecular targets involves several conceptual difficulties that have to be accommodated in the time-delay formalism introduced by Smith. These include, in addition to the presence of multiple channels, the angular dependence introduced by the directional dependence of the photoelectron on the one hand and the orientation of the molecule with respect to the laboratory-frame axes on the other hand. We first consider the case of single-photon ionization, whereby we first employ the "angular time delay" concept as introduced by Froissart, Goldberger, and Watson[36] to treat the angular dependence of molecular photoionization and discuss the procedure for averaging over the photoemission angle and the molecular orientation. Considering the fact that current experimental schemes targeting photoionization time delays involve the interaction with a second laser pulse, displaced in time relative to the ionizing extreme-ultraviolet (XUV) radiation, we next consider the case of two-photon ionization by one high-frequency (typically XUV) photon and one low-frequency (typically infrared, IR) photon. This case is relevant for experiments relying on interferometry with attosecond pulse trains (APT), also used in the reconstruction of attosecond beating by interference of two-photon transitions (RABBIT) scheme.[37] The effects of spatial averaging over the photoelectron emission angle and the molecular orientation are also discussed.

A. One-photon delays

Throughout this text, we use the method of single-center partial-wave expansion to study the photoionization of molecular targets. The formalism employed in the current section closely follows the notation employed in Ref. 41. As discussed in Ref. 42, the scattering operator, in terms of which Smith's time delay definition is constructed, can be related to the photoionization matrix element. The photoionization dipole matrix elements expressed in the length gauge are of the general form

$$I_{i,f} = \langle \Psi_{f,\vec{k}}^{(-)} | \, \vec{r} \cdot \vec{E} \, | \Psi_i \rangle \,, \tag{1}$$

where $|\Psi_i\rangle$ represents the initial-state wave function, $\vec{r}$ is the position operator, and $\vec{E}$ denotes the electric field of the laser normalized to $|\vec{E}| = 1$. In the case of linearly polarized light, Eq. (1) can be expressed in a simplified form $I_{i,f} = \langle \Psi_{f,\vec{k}}^{(-)} | \, \vec{r} \cdot \hat{n} \, | \Psi_i \rangle$, with $\hat{n}$ denoting the polarization direction. Here and in what follows, atomic units are used, unless otherwise stated. The final (residual ion + photoelectron) wavefunction is expanded into partial waves,

$$\Psi_{f,\vec{k}}^{(-)} = \sqrt{\frac{2}{\pi}} \sum_{lm} \mathrm{i}^l \Psi_{f,lm}{}^{(-)}(\vec{r}) Y_{lm}^*(\hat{k}), \tag{2}$$

where $\hat{k} \equiv (\theta_k, \phi_k)$ denotes the emission direction of the photoelectron with the asymptotic momentum k in the molecular frame of reference. Y_{lm} denotes a spherical harmonic function with a phase factor given by the Condon-Shortley convention. The partial-wave states $\Psi_{f,lm}{}^{(-)}(\vec{r})$ are energy-normalized solutions of the Lippmann-Schwinger equation defined in Ref. 40. The three components of the position operator r_μ in the molecular frame can be written explicitly in the spherical tensor form $r_\mu = \sqrt{\frac{4\pi}{3}} r Y_{1\mu}(\hat{r})$, where $\hat{r}$ denotes the direction of the position vector defined with respect to the molecular frame (MF). The electric field orientation is fixed in the laboratory frame (LF). The Z-axis of the latter is defined parallel to the polarization direction of the electric field for linearly polarized light or parallel to the propagation direction for the circular polarization. The relation between the two frames can be expressed in terms of the Euler angles ($\hat{R}_\gamma \equiv (\alpha, \beta, \gamma)$) defined in Fig. 1 that rotate the molecular frame into coincidence with the laboratory frame. The scalar product in Eq. (1) then reads (in the case of linear or circular polarization)

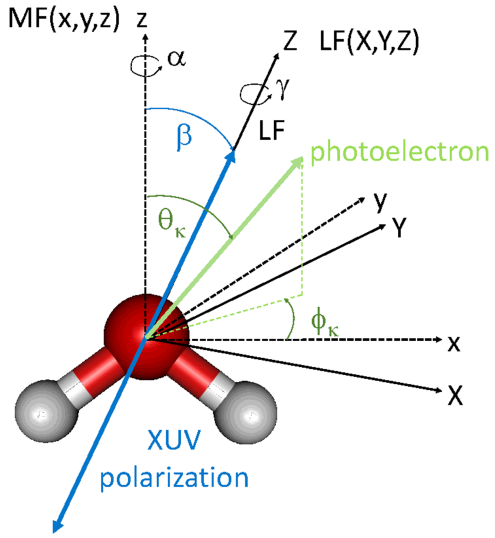

FIG. 1. Definition of the coordinate systems (molecular frame, MF, and laboratory frame, LF), the set of Euler angles $\hat{R}_\gamma = (\alpha, \beta, \gamma)$ transforming the MF into the LF, and the angles (θ_k, ϕ_k) defining photoemission.

$$\hat{\xi}_{m_p} \equiv \vec{r} \cdot \vec{E} = \sqrt{\frac{4\pi}{3}} (-1)^{m_p} r E_{-m_p} \sum_{\mu=-1}^{1} \mathcal{D}^{(1)}_{\mu m_p}(\hat{R}_\gamma) Y_{1\mu}(\hat{r}), \quad (3)$$

where $\mathcal{D}^{(j)}_{mk}$ denotes a Wigner matrix element. The symbol m_p specifies the polarization of the incident field and is given by $m_p = 0$ for linearly polarized light or $m_p = \pm 1$ for right/left circular polarization. Therefore one can expand the dipole moment $I_{i,f}$ defined in (1) as

$$I_{i,f} = \sum_{lm\mu} I_{lm\mu} Y_{lm}(\hat{k}) \mathcal{D}^{(1)}_{\mu m_p}(\hat{R}_\gamma), \quad (4)$$

where $I_{lm\mu} = \sqrt{\frac{2}{\pi}} i^{-l} (-1)^{m_p} E_{-m_p} \langle \Psi_{f,lm}{}^{(-)}(\vec{r}) | \, r_\mu \, | \Psi_i \rangle$.

Following the reasoning of Froissart, Goldberger, and Watson,[36] we can define the "angular time delay" in the context of molecular photoionization as

$$\tau_{1h\nu}(E, \hat{k}, \hat{R}_\gamma) = \frac{\partial}{\partial E} \arg \left\{ I_{i,f} \right\} = \frac{\partial}{\partial E} \arg \left\{ \sum_{lm\mu} I_{lm\mu} Y_{lm}(\hat{k}) \mathcal{D}^{(1)}_{\mu m_p}(\hat{R}_\gamma) \right\}. \quad (5)$$

Equation (5) defines a delay associated with single-photon ionization for photoemission along the direction $\hat{k}$ in the molecular frame for a particular orientation $(\hat{R}_\gamma)$ of the molecule with respect to the ionizing radiation. In the following, we refer to such quantities as emission-angle (or short angle-) and target-orientation (or short orientation-) resolved delays.

The formula given in Eq. (5) cannot be directly applied to describe an experimental situation sampling the time delay only as a function of one of the solid angles $\hat{k}$ or $\hat{R}_\gamma$ while the resolution with respect to the other is absent. The correct procedure for performing spatial averaging over $\tau(E, \hat{k}, \hat{R}_\gamma)$ must take into account the contribution of a particular emission direction to the total photoionization cross section. The method to achieve this consists of weighting the delay associated with a particular set of angles $\hat{k}$ and $\hat{R}_\gamma$ with the corresponding cross section,

$$\tau_{1h\nu}(E) = \frac{1}{8\pi^2} \int d\hat{R}_\gamma \int d\hat{k} \frac{|\sum_{lm\mu} I_{lm\mu} Y_{lm}(\hat{k}) \mathcal{D}^{(1)}_{\mu m_p}(\hat{R}_\gamma)|^2}{\sum_{lm\mu} |I_{lm\mu}|^2} \times \frac{\partial}{\partial E} \arg \left\{ \sum_{lm\mu} I_{lm\mu} Y_{lm}(\hat{k}) \mathcal{D}^{(1)}_{\mu m_p}(\hat{R}_\gamma) \right\}. \quad (6)$$

This expression defines the one-photon-ionization delay averaged over both emission angles and target orientation, i.e., the result of a non-angle-resolved measurement on a randomly oriented molecular sample. A formula similar to expression (6) for the case of scattering on a short-range potential has been derived and discussed by Nussenzveig.[43,44]

B. Two-photon delays in molecular photoionization

1. Angle- and orientation-resolved delays

In the following, we derive the two-photon matrix elements describing photoionization delays measured by a combination of XUV and IR laser pulses, typical of attosecond interferometry. In doing so, we make the following assumptions. First, the XUV photon energy Ω is assumed to be much larger than the relevant ionization potential (I_p) of the molecule. This allows one to ignore bound-state contributions to the two-photon matrix elements. Second, the intensity of the IR pulse is sufficiently low (typically $\ll 10^{12}$ W/cm^2) that multiphoton absorption of the IR plays no role. Third, ionization pathways in which the XUV photon is absorbed after the IR photon of energy ω are neglected. The two-photon ionization matrix element for a fixed-in-space target in the molecular frame (MF) is then given by

$$M(\vec{k}; \varepsilon_i + \Omega) = \frac{1}{i} \lim_{\epsilon \to 0^+} \int d\varepsilon_\nu \frac{\langle \Psi_{f,\vec{k}}{}^{(-)}(\vec{r}) | \, \hat{\xi}^{IR}_{m'_p} \, | \nu \rangle \langle \nu | \, \hat{\xi}^{XUV}_{m_p} \, | \Psi_i \rangle}{\varepsilon_i + \Omega - \varepsilon_\nu + i\epsilon}, \quad (7)$$

where $\Psi_{f,\vec{k}}{}^{(-)}(\vec{r})$ and Ψ_i are the final and initial states defined in Sec. II A, while $|\nu\rangle$ denotes an intermediate continuum state with energy ε_ν. We choose a Hartree-Fock wave function description for the initial state $|i\rangle$, as implemented in ePolyScat. We now perform a single-center partial wave decomposition of the initial-state $\Psi_i = \sum_{lm} R_{nl}(r) Y_{lm}(\hat{r})$ and intermediate-state wave functions $|\nu\rangle = \sum_{\lambda\mu} R_{\nu\lambda}(r) Y_{\lambda\mu}(\hat{r})$. Since we restrict our analysis to the case where the energy of the XUV pulse exceeds the ionization potential of the system, the summation over the intermediate states labelled ν in Eq. (7) effectively involves only partial-wave components of the intermediate continuum states accessible. In analogy to Eq. (2), $R_{\kappa\lambda}$ is also chosen such that the incoming-wave boundary conditions are satisfied. We treat the final-state wavefunction $\Psi_{f,\vec{k}}{}^{(-)}(\vec{r})$ within the frozen-core Hartree-Fock approximation, assuming a single-determinant representation of the final state in which the ionic orbitals are identical to the ones used for the description of the ground state. The photoelectron orbital corresponds to the solution of the one-electron Schrödinger equation with a potential defined by the static-exchange interaction with the molecular ion, a short-range potential term, and the Coulomb interaction.[45]

We separate the final state given by Eq. (2) explicitly in terms of radial and angular-dependent parts,

$$\Psi_{f,\vec{k}}^{(-)}(\vec{r}) = \sqrt{\frac{2}{\pi}} \sum_{LM} \mathrm{i}^L \mathrm{e}^{-\mathrm{i}\eta_L(k)} Y_{LM}^*(\hat{k}) Y_{LM}(\hat{r}) R_{kL}(r), \quad (8)$$

where the radial solution R_{kL}, corresponding to continuum momentum k, satisfies the proper incoming-wave boundary conditions, $\hat{k}$ captures the angular dependence of the ejected electron, and $\eta_L(k) = \delta_L(k) + \sigma_L(k)$ is the partial-wave phase shift that consists of a short-range ($\delta_L(k)$) and Coulomb ($\sigma_L(k)$) parts. The general expression in Eq. (7) defines the two-photon photoionization amplitude for a fixed-in-space target in the molecular frame. Thus, the transition operators $\hat{\xi}^{\mathrm{XUV/IR}}$ are tied to the MF. The polarizations of the XUV/IR fields, however, are defined with respect to the LF and correspondingly, $\hat{\xi}^{\mathrm{XUV}}/\hat{\xi}^{\mathrm{IR}}$ has to be transformed to the MF according to Eq. (3). From now on, the dependence of $M(\vec{k};\varepsilon_i+\Omega)$ on the target orientation will be denoted explicitly: $M(\vec{k};\varepsilon_i+\Omega) \rightarrow M(\vec{k};\varepsilon_i+\Omega;\hat{R}_\gamma)$. In addition, we adopt the following convention for the indices for the polarizations of the XUV/IR fields,

$$\rho', m_1 \rightarrow \mathrm{XUV}, \quad (9)$$

$$\rho, m_2 \rightarrow \mathrm{IR}. \quad (10)$$

After inserting all partial-wave expansions into (7) and evaluating the angle-dependent integrals, we obtain

$$M(\vec{k};\varepsilon_i+\Omega;\hat{R}_\gamma) = \frac{1}{\mathrm{i}} E_{-m_1}^{\mathrm{XUV}} E_{-m_2}^{\mathrm{IR}} \frac{4\pi}{3} \sqrt{\frac{2}{\pi}} (-1)^{m_1+m_2} \sum_{\substack{LM\lambda\mu \\ \rho\rho' \\ lm}} (-\mathrm{i})^L \mathrm{e}^{\mathrm{i}\eta_L(k)} \langle Y_{LM}|\, Y_{1\rho}\, |Y_{\lambda\mu}\rangle \langle Y_{\lambda\mu}|\, Y_{1\rho'}\, |Y_{lm}\rangle$$

$$\times T_{L\lambda l}(k;\varepsilon_\kappa) \mathcal{D}^{(1)}_{\rho' m_1}(\hat{R}_\gamma) \mathcal{D}^{(1)}_{\rho m_2}(\hat{R}_\gamma) Y_{LM}(\hat{k}), \quad (11)$$

where $T_{L\lambda l}(k;\varepsilon_\kappa)$ is the radial part of the two-photon transition matrix element

$$T_{L\lambda l}(k;\varepsilon_\kappa) = \sum_{\nu,\varepsilon_\nu<0} \frac{\langle R_{kL}|\, r\, |R_{\nu\lambda}\rangle \langle R_{\nu\lambda}|\, r\, |R_{nl}\rangle}{\varepsilon_i + \Omega - \varepsilon_\nu} + \lim_{\epsilon\rightarrow 0^+} \int_0^\infty \mathrm{d}\varepsilon_{\kappa'} \frac{\langle R_{kL}|\, r\, |R_{\kappa'\lambda}\rangle \langle R_{\kappa'\lambda}|\, r\, |R_{nl}\rangle}{\varepsilon_i + \Omega - \varepsilon_{\kappa'} + \mathrm{i}\epsilon}. \quad (12)$$

In the above, the symbols ν, λ, and μ denote the set of quantum numbers corresponding to the intermediate states, while κ denotes the asymptotic momentum of the electron following the XUV-induced bound-continuum transition and $\varepsilon_\kappa = \varepsilon_i + \Omega$.

We evaluate Eq. (12) in the asymptotic approximation following the work of Ref. 14. Specifically, following the derivation leading from Eq. (7) to Eq. (20) in Ref. 14, leads from our Eq. (12) to

$$T_{L\lambda l}(k;\varepsilon_\kappa) \approx \frac{1}{\sqrt{k\kappa}|\kappa-k|^2} \exp\left[-\frac{\pi Z}{2}\left(\frac{1}{\kappa}-\frac{1}{k}\right)\right] \mathrm{i}^{L-\lambda-1} \mathrm{e}^{\mathrm{i}(\eta_\lambda(\kappa)-\eta_L(k))} \frac{(2\kappa)^{\mathrm{i}Z/\kappa}}{(2k)^{\mathrm{i}Z/k}} \frac{\Gamma\left[2+\mathrm{i}Z(\kappa^{-1}-k^{-1})\right]}{(\kappa-k)^{(1/\kappa-1/k)}} \langle R_{\kappa\lambda}|\, r\, |R_{nl}\rangle\,. \quad (13)$$

Setting

$$A_{\kappa k} = \frac{1}{\sqrt{k\kappa}|\kappa-k|^2} \exp\left[-\frac{\pi Z}{2}\left(\frac{1}{\kappa}-\frac{1}{k}\right)\right] \frac{(2\kappa)^{\mathrm{i}Z/\kappa}}{(2k)^{\mathrm{i}Z/k}} \frac{\Gamma\left[2+\mathrm{i}Z(\kappa^{-1}-k^{-1})\right]}{(\kappa-k)^{1/\kappa-1/k}} \quad (14)$$

results in

$$M(\vec{k};\varepsilon_i+\Omega;\hat{R}_\gamma) = -E_{-m_1}^{\mathrm{XUV}} E_{-m_2}^{\mathrm{IR}} \frac{4\pi}{3} \sqrt{\frac{2}{\pi}} (-1)^{m_1+m_2} A_{\kappa k} \sum_{\substack{LM\lambda\mu \\ \rho\rho' \\ lm}} (\mathrm{i})^{-\lambda} \mathrm{e}^{\mathrm{i}\eta_\lambda(\kappa)} \langle R_{\kappa\lambda}|\, r\, |R_{nl}\rangle \langle Y_{\lambda\mu}|\, Y_{1\rho'}\, |Y_{lm}\rangle \langle Y_{LM}|\, Y_{1\rho}\, |Y_{\lambda\mu}\rangle$$

$$\times \mathcal{D}^{(1)}_{\rho' m_1}(\hat{R}_\gamma) \mathcal{D}^{(1)}_{\rho m_2}(\hat{R}_\gamma) Y_{LM}(\hat{k}). \quad (15)$$

The quantity $A_{\kappa k}$ can be identified as an IR-induced, "continuum-continuum" part of the two-photon amplitude as it does not depend on the target structure within the asymptotic approximation used here. By comparison with the definition of $I_{lm\mu}$ after Eq. (4), one can also identify the photoionization matrix element corresponding solely to the XUV-absorption step

$$I_{\lambda\mu\rho'} := (-1)^{m_1} E_{-m_1}^{\mathrm{XUV}} \sqrt{\frac{4\pi}{3}} (\mathrm{i})^{-\lambda} \mathrm{e}^{\mathrm{i}\eta_\lambda(\kappa)} \sum_{lm} \langle R_{\kappa\lambda}|\, r\, |R_{nl}\rangle \langle Y_{\lambda\mu}|\, Y_{1\rho'}\, |Y_{lm}\rangle. \quad (16)$$

We note that Eq. (16) corresponds to the complex-conjugate of the PI-matrix element defined in Ref. 41. With these auxiliary definitions, the matrix element

$$M(\vec{k};\varepsilon_i+\Omega;\hat{R}_\gamma) = \sqrt{\frac{4\pi}{3}} (-1)^{m_2+1} E_{-m_2}^{\mathrm{IR}} A_{\kappa k} \sum_{\substack{LM \\ \rho\rho' \\ \lambda\mu}} I_{\lambda\mu\rho'} \langle Y_{LM}|Y_{1\rho}\,|Y_{\lambda\mu}\rangle \mathcal{D}^{(1)}_{\rho' m_1}(\hat{R}_\gamma) \mathcal{D}^{(1)}_{\rho m_2}(\hat{R}_\gamma) Y_{LM}(\hat{k}) \quad (17)$$

can be cast in a concise form

$$M(\vec{k};\varepsilon_i+\Omega;\hat{R}_\gamma) = A_{\kappa k} \sum_{LM} b_{LM}^{m_1,m_2}(\hat{R}_\gamma) Y_{LM}(\hat{k}), \quad (18)$$

where the orientation-dependent coefficients $b_{LM}^{m_1,m_2}(\hat{R}_\gamma)$ are defined as

$$b_{LM}^{m_1,m_2}(\hat{R}_\gamma) = \sqrt{\frac{4\pi}{3}}(-1)^{m_2+1}E_{-m_2}^{\mathrm{IR}} \sum_{\substack{\rho\rho'\\ \lambda\mu}} I_{\lambda\mu\rho'} \langle Y_{LM}|Y_{1\rho}\,|Y_{\lambda\mu}\rangle \mathcal{D}^{(1)}_{\rho' m_1}(\hat{R}_\gamma)\mathcal{D}^{(1)}_{\rho m_2}(\hat{R}_\gamma)$$

$$= (-1)^{m_\mathrm{p}+\rho+1}E_{-m_2}^{\mathrm{IR}} \sum_{\substack{\rho\rho'\\ \lambda\mu}} \sqrt{\tfrac{2L-1}{2\lambda+1}}\langle L010|\lambda 0\rangle\langle LM1-\rho|\lambda\mu\rangle I_{\lambda\mu\rho'}\mathcal{D}^{(1)}_{\rho' m_1}(\hat{R}_\gamma)\mathcal{D}^{(1)}_{\rho m_2}(\hat{R}_\gamma), \tag{19}$$

where the symbol $\langle ....|..\rangle$ denotes a Clebsch-Gordan coefficient.

In the following, we discuss the two-photon delays accessible in a RABBIT measurement. Up to this point, our equations are valid for both linearly and circularly polarized radiations and arbitrary relative polarizations of XUV and IR. For simplicity, we now restrict the polarizations of XUV and IR fields to be linear and parallel to each other, i.e., $m_1 = m_2 = 0$ and the superscripts in the $b_{LM}^{m_1,m_2}$-coefficients will be omitted for brevity. The angle- and orientation-resolved intensity of a photoelectron sideband corresponding to energy $2q\omega$ ($q \in \mathbb{N}$) created in an attosecond interferometry experiment is given by

$$\frac{\mathrm{d}^2P_{2q}}{\mathrm{d}\hat{k}\,\mathrm{d}\hat{R}_\gamma} \propto |M^{(2q-1)} + M^{(2q+1)}|^2 = |M^{(2q-1)}|^2 + |M^{(2q+1)}|^2 + 2|M^{(2q-1)}||M^{(2q+1)}|\cos\left[\arg\left\{M^{(2q-1)*}M^{(2q+1)}\right\}\right]. \tag{20}$$

Here and in what follows, the label $(2q \pm 1)$ attached to a particular symbol indicates that the corresponding quantity has to be evaluated at a value $\kappa_\pm \equiv \sqrt{2((2q\pm1)\omega - I_\mathrm{p})}$ for the asymptotic momentum of the intermediate photoelectron state. The final asymptotic momentum of the electron after the IR-induced transition is given by $k = \sqrt{2(2q\omega - I_\mathrm{p})}$.

The angle- and orientation-resolved delay in the finite-difference approximation[14] reads

$$\tau(2q,\hat{k},\hat{R}_\gamma) = \frac{1}{2\omega}\arg\left(M^{(2q-1)*}M^{(2q+1)}\right), \tag{21}$$

where

$$M^{(2q-1)*}M^{(2q+1)} = A_{\kappa_- k}^{(2q-1)*}A_{\kappa_+ k}^{(2q+1)} \sum_{\substack{LM\\ L'M'}} b^*_{L'M';(2q-1)}(\hat{R}_\gamma) \times b_{LM;(2q+1)}(\hat{R}_\gamma)Y^*_{L'M'}(\hat{k})Y_{LM}(\hat{k}). \tag{22}$$

This quantity contains the maximal available information about the attosecond photoionization dynamics. The delay can accordingly be written as a sum of two terms,

$$\tau(2q,\hat{k},\hat{R}_\gamma) = \tau_{\mathrm{cc}}(2q) + \tau_{\mathrm{mol}}(2q,\hat{k},\hat{R}_\gamma). \tag{23}$$

The structure of Eq. (23) shows that measurements of molecular photoionization delays by attosecond interferometry, just as their atomic counterparts, can be interpreted in terms of a continuum-continuum contribution (or measurement-induced delay),[5,14]

$$\tau_{\mathrm{cc}}(2q) = \frac{1}{2\omega}\arg\left[A_{\kappa_- k}^{(2q-1)*}A_{\kappa_+ k}^{(2q+1)}\right], \tag{24}$$

which only depends on the photon energies, i.e., the harmonic orders. However, the angular momentum addition describing the interaction with the IR photon leads to a non-trivial modification of the angle-dependence of the delays that we factorize into a molecule-specific contribution that can be expressed as[20]

$$\tau_{\mathrm{mol}}(2q,\hat{k},\hat{R}_\gamma) = \frac{1}{2\omega}\arg\left[\sum_{\substack{LM\\ L'M'}} Y^*_{L'M'}(\hat{k})Y_{LM}(\hat{k})b^*_{L'M';(2q-1)}(\hat{R}_\gamma) \times b_{LM;(2q+1)}(\hat{R}_\gamma)\right]. \tag{25}$$

The reason for this additional complexity as compared to atoms lies in the fact that molecules lack spherical symmetry and therefore several (in principle, infinitely many) partial waves are required to describe molecular photoionization. Although molecular photoionization delays can, in principle, be measured with angular resolution for fixed-in-space molecules, such experiments have not been reported to date. We therefore now discuss the effects of angular and target-orientation averaging.

2. Effect of averaging over emission angle and target orientation

In the following, we describe several possible configurations of experimental interest. We first introduce the effect of averaging over the emission angle $\hat{k}$ of the photoelectron. Equation (20) is easily uniformly averaged over $\hat{k}$ by exploiting the orthonormality of the spherical harmonics (see Eq. (22)) leading to

$$\tau(2q,\hat{R}_\gamma) = \tau_{\mathrm{cc}}(2q) + \frac{1}{2\omega}\arg\left[\sum_{LM} b^*_{LM;(2q-1)}(\hat{R}_\gamma) \times b_{LM;(2q+1)}(\hat{R}_\gamma)\right]. \tag{26}$$

This quantity represents the delay measured from perfectly oriented molecules by averaging over the emission angle of the photoelectron.

Measurements of molecular photoionization delays have so far only been reported for unaligned samples.[20] This

situation is described by additionally averaging over all molecular orientations leading to

$$\tau(2q) = \tau_{cc}(2q) + \frac{1}{2\omega}\arg\left[\sum_{LM}\int d\hat{R}_\gamma b^*_{LM;(2q-1)}(\hat{R}_\gamma) \times b_{LM;(2q+1)}(\hat{R}_\gamma)\right]. \quad (27)$$

Molecular photoionization delays could also be measured by aligning and orienting molecules in space using non-resonant laser pulses[46–49] or by post-selection in coincidence/covariance experiments for cases where dissociative photoionization pathways can be cleanly separated and the axial recoil approximation is valid. In all such cases, averaging must be performed over a characteristic axis distribution $A(\hat{R}_\gamma)$ and the corresponding delays are given by

$$\tau(2q) = \tau_{cc}(2q) + \frac{1}{2\omega}\arg\left[\sum_{LM}\int d\hat{R}_\gamma A(\hat{R}_\gamma) \times b^*_{LM;(2q-1)}(\hat{R}_\gamma) b_{LM;(2q+1)}(\hat{R}_\gamma)\right]. \quad (28)$$

Finally, a measurement of angle-resolved delays could be performed for a randomly aligned molecular sample. This situation is described by uniformly averaging over $\hat{R}_\gamma$ only, but not over $\hat{k}$,

$$\tau(2q,\hat{k}) = \tau_{cc}(2q) + \frac{1}{2\omega}\arg\left[\sum_{\substack{LM\\L'M'}} Y^*_{L'M'}(\hat{k}) Y_{LM}(\hat{k}) \times \int d\hat{R}_\gamma b^*_{L'M';(2q-1)}(\hat{R}_\gamma) b_{LM;(2q+1)}(\hat{R}_\gamma)\right]. \quad (29)$$

C. Comparison to the atomic case

At this point, it is pertinent to outline the differences between the molecular case discussed so far and the result for an atomic system. Specifically, we compare Eq. (15) from this article with Eq. (24) of Ref. 14.

The first difference arises from the lack of spherical symmetry of molecules and applies both in the molecular and in the laboratory frames. The absence of spherical symmetry requires the summation over ℓ, the angular-momentum quantum number of the partial waves involved in the expansion of the initial bound state. In contrast, the initial bound state of atoms can be described by a single value of ℓ. Additionally, exploiting the Fano propensity rule,[50] which states that the transition $\ell \to \ell + 1$ strongly dominates over the transition $\ell \to \ell - 1$, the phase of the two-photon matrix elements for atoms can be reduced to a sum containing the scattering phase $\eta_{\ell+1}(\kappa)$ and the cc-phase (the argument of Eq. (14) in this article), as done in Ref. 5. Consequently, the two-photon delay accessible in angle-integrated RABBIT measurements of atoms can be written as

$$\tau(2q) = \tau_{cc}(2q) + \tau_{1h\nu}(2q), \quad (30)$$

i.e., as a sum of a one-photon-ionization delay (the Wigner delay) and a continuum-continuum delay. In the case of molecules, this separability does not exist in the same form because the initial state cannot be represented by a single partial wave. Multiple partial waves are required to represent the initial state, therefore multiple partial waves are also required to represent the intermediate (one-photon-ionized) state, which leads to interference phenomena, e.g., between the pathways $\ell \to \ell + 1$ and $\ell + 2 \to \ell + 1$. Additional interferences occur at the level of the two-photon transitions, e.g., between $\ell \to \ell + 1 \to \ell$ and $\ell + 2 \to \ell + 1 \to \ell$.

For these reasons, the two-photon delays in molecular photoionization cannot be written as a sum of a one-photon-ionization delay and a universal continuum-continuum contribution. In other words, there is no simple additive relation between $\tau(2q,\hat{k},\hat{R}_\gamma)$ and $\tau_{1h\nu}(2q,\hat{k},\hat{R}_\gamma)$ in the molecular case. However, owing to the independence of τ_{cc} on the values of the angular-momentum quantum numbers, one can still isolate a "continuum-continuum contribution" (see Eq. (23)), but the residual τ_{mol} has no simple relation to $\tau_{1h\nu}$. Consequently, the effect of the probing IR field on the delays measured in the molecular case cannot be represented by a simple, universal quantity. Instead, one has to first evaluate Eq. (19), followed by Eqs. (25)–(29), depending on the case of experimental interest.

The second difference to the atomic case is the dependence of all matrix elements on the orientation of the target molecule, i.e., the dependence on the Euler angles $\hat{R}_\gamma$, which is explicitly given in the preceding equations. The dependence of the delays on $\hat{R}_\gamma$ is very pronounced, as we show below, and it plays a crucial role in averaging over the axis distribution, which is relevant for all experiments. The non-trivial aspect of the orientational-averaging arises from the fact that Eqs. (27)–(29) represent coherent integrals over complex quantities. This fact can completely change the energy-dependence of $\tau_{mol}(2q)$, as we illustrate in Section III C. We show that the coherent averaging over molecular orientations can shift the position of the maximal delay caused by a shape resonance by ∼7 eV when comparing the one-photon-ionization delays $\tau_{1h\nu}$ with the molecular part of the two-photon delays τ_{mol}.

III. APPLICATIONS

We apply the expressions derived in Sec. II B to the case of two polyatomic molecules that have recently been investigated experimentally using attosecond interferometry, i.e., N_2O and H_2O.[20] The scattering calculations were performed numerically using ePolyScat,[38,39] which is based on the Schwinger variational principle.[40] The initial-state single-determinant wavefunction Ψ_i was obtained from a Hartree-Fock quantum chemistry calculation using the 3-21G basis set and bond lengths of R(N–N) = 1.207 Å and R(N–O) = 1.237 Å in the case of N_2O. In the case of H_2O, the cc-pVTZ basis set was used with bond lengths of R(O–H) = 0.9578 Å and a bond angle of θ(HOH) = 104.5 °. In both cases, we employed the frozen-nuclei approximation and performed the scattering calculation keeping fixed bond distances and angles. The choice of a rather small basis in the case of N_2O is justified by the fact that the scattering calculations correctly reproduce the

experimentally observed photoionization cross sections and the asymmetry parameters (see the supplementary material of Ref. 20). The comparison of calculated and observed photoionization cross sections indeed validates the magnitude of the photoionization dipole-matrix elements. The comparison of photoelectron angular distributions additionally validates the accuracy of the relative phases of different partial-wave channels belonging to the same final electronic state of the cation. Relative delays in photoionization[20] are moreover sensitive to the relative phases of photoelectron continua belonging to different final states of the cation, which constitutes an additional motivation for measuring and calculating such delays.

A. Delays in one-photon ionization

We first illustrate the angle- and orientation-resolved delays in one-photon ionization, as defined by Eq. (5). These delays for ionization from the $\tilde{X}^1\Sigma^+$ electronic ground state of N_2O to the first electronically excited state $\tilde{A}^{+2}\Sigma^+$ of N_2O^+ are shown in Fig. 2 for a molecule aligned parallel ($(\alpha = 0, \beta = 0, \gamma = 0)$, panel (a)) or perpendicular ($(\alpha = 0, \beta = \pi/2, \gamma = 0)$, panel (b)) to the polarization of the ionizing radiation. These choices of the Euler angles enable us to isolate the parallel transition to the σ continuum from the perpendicular one, associated with the continuum of π-symmetry. The cylindrical symmetry of the N_2O system lifts the dependence of the angle-resolved time delay on the azimuthal photoemission angle ϕ. Figure 2 shows the delays as a function of the molecular-frame photoemission direction, quantified by the polar angle θ measured from the internuclear axis.

The same quantities are illustrated in Fig. 3 for the case of one-photon ionization from the $\tilde{X}^1A_1$ electronic ground state of H_2O to the $\tilde{A}^{+\,2}A_1$ electronically excited state of H_2O^+. The accessible continua have a_1 and b_1 symmetries in this case. The azimuthal angle ϕ has been set to 0 in this case. Note the use of different color scales in Figs. 2 and 3, motivated by the fact that the delays are much smaller in magnitude in the case of H_2O than in N_2O.

At low photon energies, the angle-resolved delay maps of both N_2O and H_2O are dominated by large positive delays due to the attractive nature of the Coulomb potential, the regions around 2.5–3 rad in N_2O and the narrow region centered around 1 rad in H_2O being exceptions to this trend. The most striking feature that becomes apparent when comparing these results is the richness of the angular structures in the angle-resolved photoionization time delays of

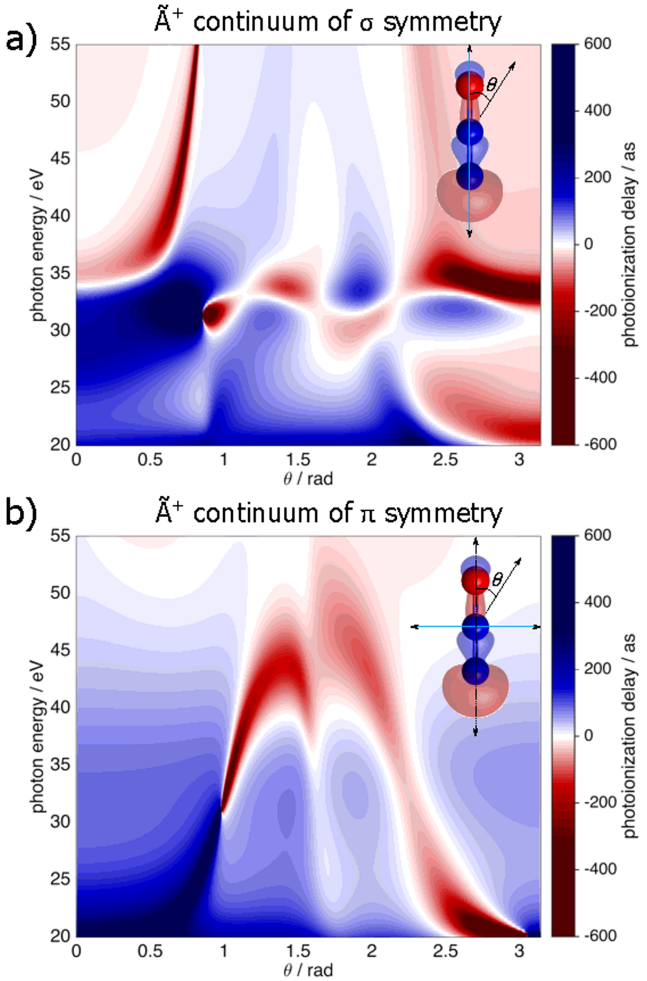

FIG. 2. Delays in the one-photon ionization of N_2O to the $\tilde{A}^{+\,2}\Sigma^+$ state of N_2O^+, given in the molecular frame. (a) XUV polarization parallel to the molecular axis, (b) XUV polarization perpendicular to the molecular axis.

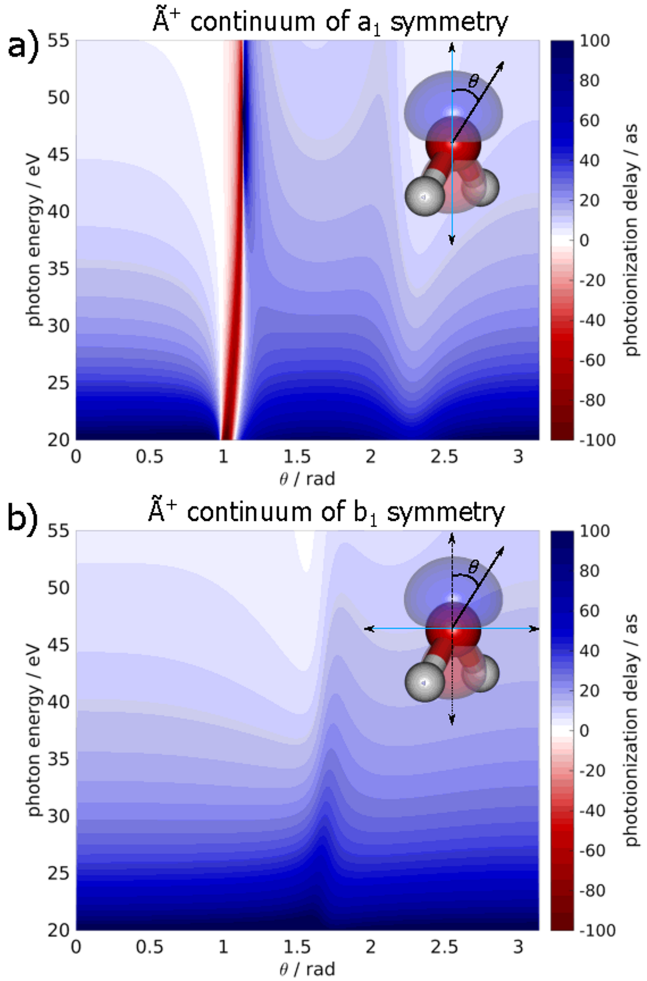

FIG. 3. Delays in the one-photon ionization of H_2O to the $\tilde{A}^{+\,2}A_1$ state of H_2O^+, given in the molecular frame. (a) XUV polarization parallel to the principal axis, (b) XUV polarization perpendicular to the principal axis.

N_2O and the contrasting simplicity of the same quantities in H_2O.

The rich angular structure in the case of N_2O is partially attributed to shape resonances embedded in the photoionization continua of this molecule. Previous work[51–58] in the realm of photoelectron spectroscopy has revealed a weak shape resonance associated with the $7\sigma \rightarrow k\sigma$ channel in N_2O located in the region around photon energies of 32 eV.[55] Notably, the single-photon angle-resolved time delay of the parallel transition in N_2O (panel (a) of Fig. 2) is characterized by large values (in terms of absolute amplitude) and rapid variations as a function of the photoemission direction θ in this particular region (30–35 eV). These delays are first strongly positive for small angles (0.5–0.8 rad), then change rapidly in the region from 1 to 2.4 rad, and finally reach large negative values as evident from the "ridge" located at $\theta > 2.5$ rad. With increasing energies, the angular dependence of the delays becomes smoother, the sole exception being a narrow feature ($\theta \approx 0.5 - 0.6$ rad) associated with strongly negative values of the delays. The transition to the π-continuum shown in Fig. 2(b) contains a very broad and weak shape resonance centered at around 38 eV.[55] It is presumably the broadness of this resonance that leads to smearing out of the angular features in this region. Regions of large positive, abruptly followed by large negative delays are observed at $\theta \approx 1$ rad and around 35 eV; this feature becoming progressively less negative and moving towards higher angles with increasing energy.

In contrast to the non-uniform behaviour of the time delays in both channels of the $\tilde{A}^+\,^2\Sigma^+$-continuum of N_2O, the angular maps for the corresponding photoionization transitions in H_2O are essentially monotonic. The predominantly negative delays and the relatively subtle angular dependencies (at least in Fig. 3(b)) reflect the dominant effect of the attractive Coulomb potential on the photoionization delays. The main exception to this trend is the narrow negative ridge centered at $\theta \approx 1$ rad extending through the entire energy range in Fig. 3(a). This structure has an intuitive interpretation. Since the $\tilde{A}^+\,^2A_1$ state of H_2O^+ is well described by an electron being removed from the $3a_1$ orbital of dominant atomic p-character (see inset of Fig. 3(a)), the continuum is dominated by s- and d-waves. Since s-waves are spherically symmetric, whereas the d-waves accessible by symmetry change sign at the magic angle ($\theta \approx 54.7° \approx 1.05$ rad), the total photoionization matrix elements to the continuum of a_1 symmetry display a rapid variation of their amplitude and phase around 1 rad, which manifests itself as a local extremum in the photoionization delays. Photoionization by radiation polarized perpendicular to the C_2 symmetry axis leads to the continuum of b_1 symmetry (Fig. 3(b)), dominated by d-waves of d_{xz} symmetry (where z is the direction of the C_2 axis and x the polarization direction of the ionizing radiation). Since we have restricted our analysis to the value $\phi = 0$ for the emission direction, the contribution from the b_2 continuum accessible via a transition polarized along the molecule-fixed y-axis can be neglected as the dominant d_{yz} waves have a nodal surface at this value of the azimuthal angle. The photoionization delays in the b_1 channel therefore display a rapid variation around $\theta \approx 90° \approx \pi/2$ rad, where the matrix elements to the d_{xz} continuum change sign, but not around $\theta \approx 1$ rad, where the matrix elements vary smoothly with θ and energy, leading to very small angle-dependent delays.

Having outlined the relationship between the angle-resolved molecular delays and the structure of the corresponding continuum for one particular target orientation, we now turn to the effect of angular averaging over the photoemission and/or orientation directions. Figure 4 shows the delays for N_2O (after coherently adding the contributions of the parallel and perpendicular transitions) as a function of the emission angle $\hat{k} \equiv \theta$ after averaging over the Euler angles (panel (a)), or, alternatively, as a function of the Euler angle β (the polar angle between the molecular and lab frames) after averaging over all emission directions (panel (b)). In general, the integration with respect to either direction leads to a decrease in the absolute magnitude of the time delays, which motivates the use of a new color scale in Fig. 4. The averaging over the direction of photoemission leads to an overall smearing and smoothing of the previously discussed features. However, the $7\sigma \rightarrow k\sigma$-shape-resonance region remains identifiable as an area (around 33 eV) of locally increased photoionization delays for the entire range of β. Interestingly, the orientation-averaged, photoemission-angle-resolved delays displayed in panel (b) still feature a region with remarkably large

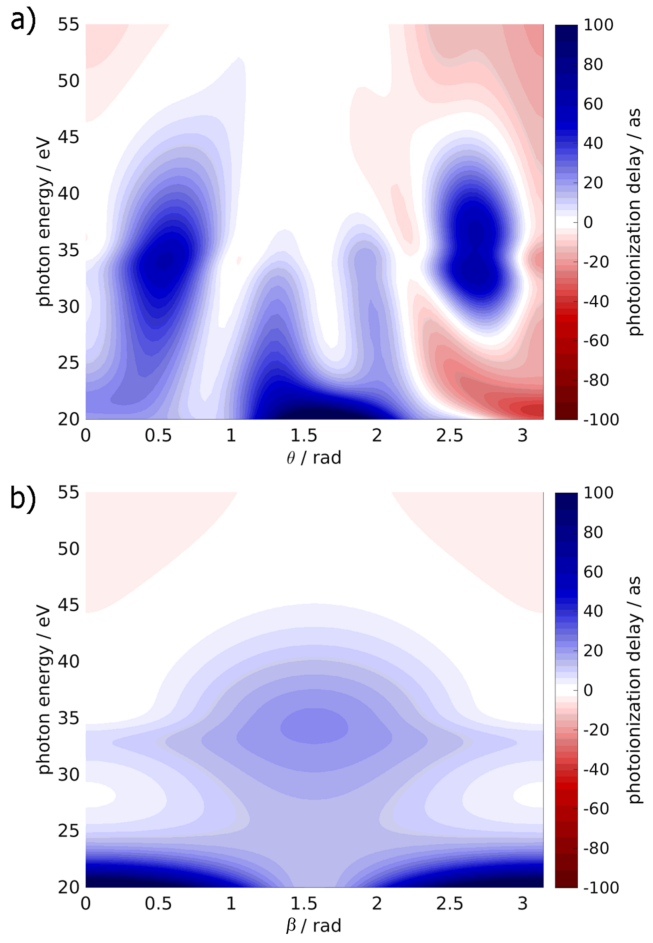

FIG. 4. (a) Photoemission-angle-resolved one-photon photoionization delays of N_2O to the $\tilde{A}^+\,^2\Sigma^+$-state of N_2O^+, averaged over the molecular orientations according to Eq. (6). (b) Orientation-resolved one-photon photoionization delays for the same system, averaged over the photoemission direction and reported as a function of the Euler angle β.

positive values (localized at angles θ between 0.2 and 0.6 rad and 2.4–2.8 rad) close to the above discussed shape resonance and extending towards the region near 40 eV. The comparison of Figs. 2 and 4 shows that the orientational averaging preserves a substantial amount of the time-delay structure observed in the molecular frame. However, the quantity represented in Fig. 4 is not related to the experimentally measured delays in a simple way, as discussed in Section II C.

B. Delays in two-photon ionization

Attosecond interferometry relies on the use of synchronized XUV and IR pulses and consists of measuring the phase of the intensity oscillations of sidebands created by $1+1'$ two-color photoionization. The effective photoionization delays obtained in such measurements are defined by Eq. (21). These effective photoionization delays, just like the one-photon-ionization delays, have a non-trivial dependence on the angles $\hat{k}$ and $\hat{R}_\gamma$. Since these delays can however be written as a sum of an angle-independent term (Eq. (24)) and an angle-dependent part ($\tau_{\mathrm{mol}}(2q, \hat{k}, \hat{R}_\gamma)$, Eq. (25)), we now illustrate the latter quantity for values of $\hat{R}_\gamma$ selected by symmetry. In the following, the IR photon energy is chosen to be 1.55 eV, corresponding to the most-frequently used central wavelength of 800 nm, and the XUV photon energy is treated as a continuous variable.

In analogy to Sec. III A, we show in Figs. 5 and 6 the emission-angle-resolved two-photon delays for the transition $\tilde{X}\,{}^1\Sigma^+\,N_2O \rightarrow \tilde{A}^+\,{}^2\Sigma^+\,N_2O^+$ and $\tilde{X}\,{}^1A_1\,H_2O \rightarrow \tilde{A}^+\,{}^2A_1\,H_2O^+$ for $\beta = 0$ and $\beta = \pi/2$. The general features of the one-photon angular-dependent maps are preserved in the maps for the two-photon transitions. Both the sign and the magnitudes of the delays are comparable, but a detailed inspection of the results reveals many differences. For example, a wide area of negative delays appears in Fig. 5(a) between $\theta = 1.6$ and 2 rad below energies of ~29 eV, where the delays in Fig. 2(a) are positive. Similarly, a region of negative delays also appears between $\theta = 0.8$ and 1 rad between photon energies of 22 and 28 eV. Additionally, the angular variation of the one- and two-photon-ionization delays is also quite different, as illustrated by the comparison of the central regions of positive delay in Figs. 2(a) and 5(a). Turning to Fig. 5(b), we find more subtle changes as compared to Fig. 2(b). However, a new region of positive delays appears below $\theta = 0.2$ rad, and the overall range of the delays is significantly reduced in Fig. 5(b) compared to Fig. 2(b). A similar trend is also observed when comparing

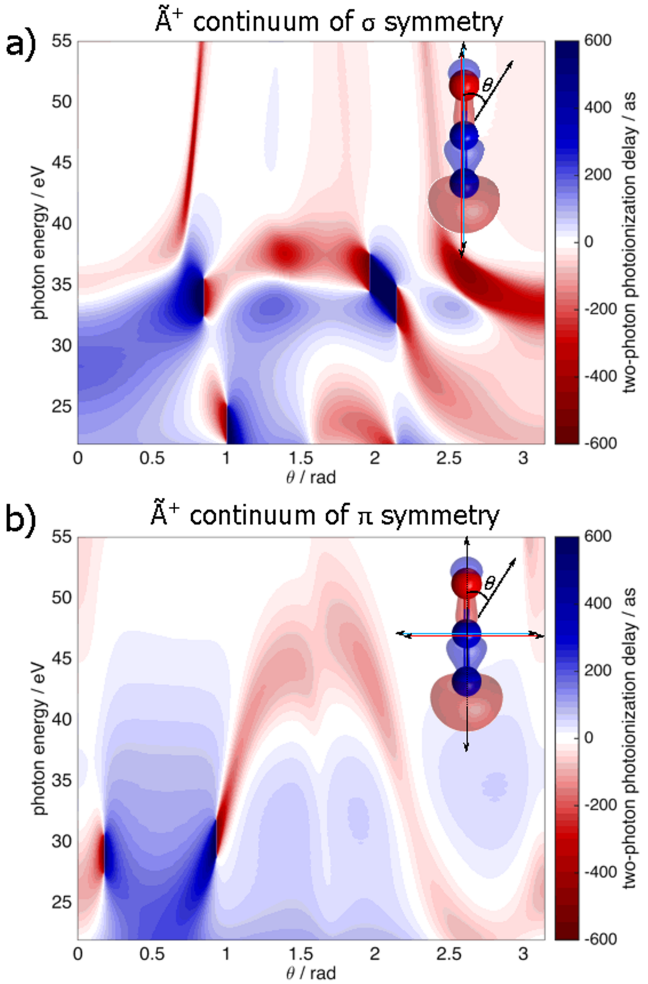

FIG. 5. Two-photon ionization delays (τ_{mol}, as defined by Eq. (25)) of N_2O to the $\tilde{A}^+\,{}^2\Sigma^+$ state of N_2O^+, given in the molecular frame. (a) XUV and IR polarizations are both parallel to the molecular axis, (b) XUV and IR polarizations are both perpendicular to the molecular axis.

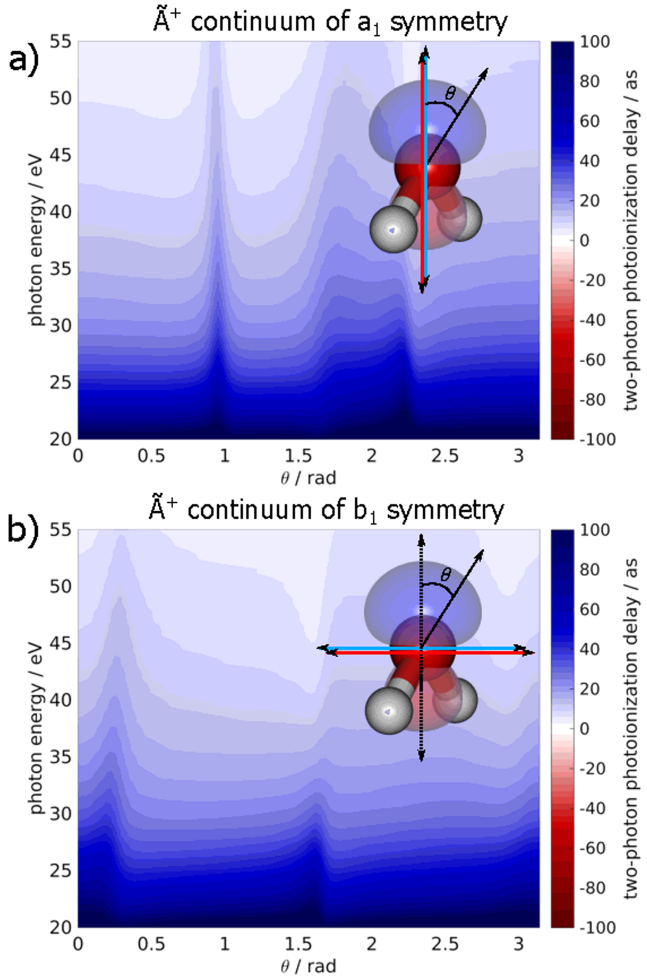

FIG. 6. Two-photon ionization delays (τ_{mol}, as defined by Eq. (25)) of H_2O to the $\tilde{A}^+\,{}^2A_1$ state of H_2O^+, given in the molecular frame. (a) XUV and IR polarizations are both parallel to the molecular axis, (b) XUV and IR polarizations are both perpendicular to the molecular axis.

Figs. 3 and 6. The main features are qualitatively very similar. However, the sharp ridge of negative delays for $\theta \approx 1$ rad in Fig. 3(a) is replaced by a line of weakly positive delays in Fig. 6(a). The results shown in Figs. 3(b) and 6(b) are even more similar, except for the appearance of an additional ridge of small positive delays around $\theta \approx 0.2$ rad in Fig. 6(b).

C. Comparison of angle-averaged delays in one- and two-photon ionization

Sections III A and III B have illustrated the angle and orientation dependencies of the one- and two-photon-ionization delays. This comparison has shown that the angle-dependent features of the one-photon-ionization delays are qualitatively retained in the two-photon-ionization delays but that the two types of delays differ on a quantitative level. This insight will be useful and important in future angle-resolved measurements of molecular photoionization delays. We now compare the effects of angular or orientational averaging on the one- and two-photon-ionization delays on a more quantitative level.

We first compare in Fig. 7 the one- and two-photon-ionization delays for selected orientations (β values) of N_2O after averaging over the direction of photoemission (θ). All delays display a local maximum which shifts from 32.8 eV at $\beta = 0$ rad to 34.5 eV at $\beta = \pi/2$ rad in panel (a) and from 32.5 eV to 33.0 eV in panel (b). The location of this maximum coincides well with the position of the shape resonance discussed above. Although the positions of the maxima are similar, we note that the magnitude of the delays and their energy dependencies differ substantially between the one- and two-photon-ionization delays. This is a consequence of the non-universal effect of the probe photon on molecular two-photon-ionization delays.

In the second step, we now investigate the even more significant impact of the additional averaging over the target orientation. Figure 8 shows the corresponding one- and two-photon-ionization delays for the cases of N_2O and H_2O discussed in this article. The solid blue curve represents the one-photon-ionization delay of N_2O following complete angular averaging. It displays a pronounced local maximum at a photon energy of 33 eV, i.e., again in the region of the shape resonance. The angle- and orientation-averaged one-photon-ionization delays result from an incoherent averaging over their only angle-averaged counterparts (cf. Fig. 7(a)). The effect of orientational averaging on one-photon-ionization delays in this case therefore mainly consists of changing their magnitude. In contrast to this, orientational averaging has a much more dramatic effect on the two-photon-ionization delays. Comparing the red curve in Fig. 8(a) with the red curves in Fig. 7(b), we find that the maximum in the orientation-averaged two-photon-ionization delays is shifted downwards by ~7 eV to a photon energy of ~26 eV.

The seemingly surprising difference in the effects of orientational averaging on the one- and two-photon-ionization delays can be understood by the inspection of Eqs. (6) and (19). Whereas the orientation dependence of the one-photon-ionization delays arises from the presence of a single Wigner rotation-matrix element, the orientation dependence of the two-photon matrix element involves a sum over products of two Wigner rotation-matrix elements. This more complex dependence enables much richer interference phenomena to take place in the angle-averaging process. In the present case, we find that the orientational average can shift the position of the maxima in the two-photon-ionization delays by a substantial amount. The generality of this result will be investigated in future work.

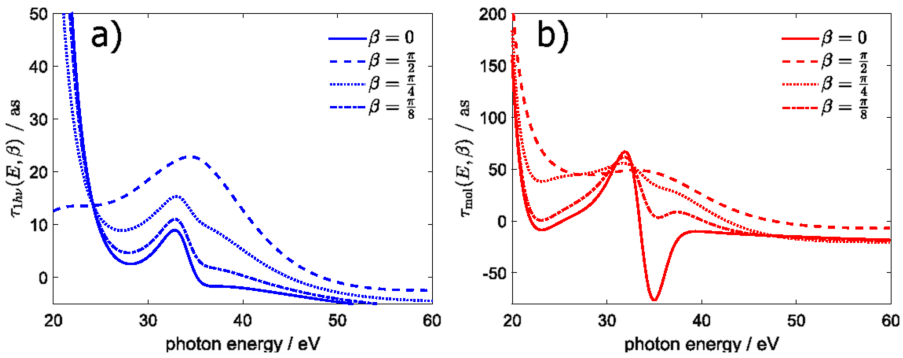

FIG. 7. Comparison of one-photon-ionization (a) and two-photon-ionization delays (b) for selected molecular orientations (β given in the legend, results integrated over γ) for the case of the photoionizing transition $\tilde{X}\,^1\Sigma^+\,N_2O \rightarrow \tilde{A}^+\,^2\Sigma^+\,N_2O^+$ after averaging over the photoemission direction.

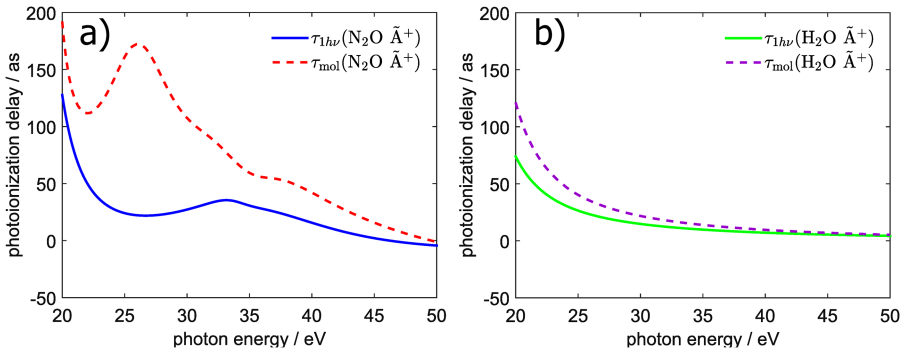

FIG. 8. Comparison of one-photon -ionization (solid lines) and two-photon-ionization (dashed lines) delays for the two investigated systems ((a) $\tilde{X}\,^1\Sigma^+\,N_2O \rightarrow \tilde{A}^+\,^2\Sigma^+\,N_2O^+$ and (b) $\tilde{X}\,^1A_1\,H_2O \rightarrow \tilde{A}^+\,^2A_1\,H_2O^+$) after averaging over both photoemission direction and molecular orientation.

In the case of the water molecule, illustrated in Fig. 8(b), the differences between angle-averaged one- and two-photon delays are much less pronounced, which is most likely a consequence of the lack of the structure in the photoionization continuum of H_2O considered here. Both the one- and the two-photon-ionization delays monotonically decrease as a function of energy but the two-photon delays are slightly lower in magnitude than the one-photon case. Finally, we point out that the theoretical results described in this article are supported by the experimental results reported in Ref. 20.

IV. CONCLUSIONS

In this article, we have developed the theory for calculating one- and two-photon ionization delays of arbitrary molecules using *ab initio* quantum scattering calculations. Starting with an expression connecting the single-photon photoionization matrix element and the concept of "time delay" as employed in the context of the analysis of scattering phenomena, the time delays encountered in molecular photoionization phenomena were found to be subject to pronounced variations as a function of energy, photoemission direction, and target orientation. The highly anisotropic nature of the scattering potential experienced by the outgoing wavepacket gives rise to pronounced angular dependences of the photoionization time delay as revealed by both emission- and orientation-direction-resolved angular maps. By comparing the location of these features with results of spectral measurements, in particular photoelectron spectroscopy, and results from molecular photoionization calculations, we were able to relate the angular structures to the presence of shape resonances in the valence continuum. This fact is clarified by comparing the one-photon delays in the two molecules N_2O and H_2O for photoionization initiating from the electronic ground states of the neutral species and terminating in the first excited electronic states of the cation. We find that the energy positions associated with the presence of shape resonances in the $7\sigma \rightarrow k\sigma$ and $7\sigma \rightarrow k\pi$-channels lead to rapid variations of the time delay as a function of angle in the case of N_2O, a situation that contrasts with the rather monotonic angular dependence of the time delays in the water molecule. These features were found to be very sensitive to averaging effects, both with respect to the photoemission and target-orientation directions. We then provided a formalism for calculating the two-photon matrix elements that are relevant to interferometric measurements where the delays associated with the XUV-mediated photoionization step are entangled with the contributions of IR-induced transitions coupling different continua. Photoemission- and orientation-direction averaging can have significant effects on the observed total delays, leading even to an energy shift of the local maximum of the delay, associated with the position of a shape resonance, as demonstrated in the case of N_2O. In principle, the formalism presented in this article can easily be applied to other molecular targets, including more complex systems such as large polyatomic molecules or clusters, provided that the scattering matrix elements as defined by Eq. (1) are available. Our work thus establishes the foundation for the calculation and theoretical analysis of the photoionization of molecules on attosecond time scales. Interesting applications and refinements of this work will include the analysis of electron correlation phenomena in molecular photoionization.

ACKNOWLEDGMENTS

We gratefully acknowledge funding from an ERC Starting Grant (Contract No. 307270-ATTOSCOPE) and the NCCR-MUST, a funding instrument of the Swiss National Science Foundation.

[1] A. L. Cavalieri, N. Muller, T. Uphues, V. S. Yakovlev, A. Baltuska, B. Horvath, B. Schmidt, L. Blumel, R. Holzwarth, S. Hendel, M. Drescher, U. Kleineberg, P. M. Echenique, R. Kienberger, F. Krausz, and U. Heinzmann, Nature **449**, 1029 (2007).
[2] R. Locher, L. Castiglioni, M. Lucchini, M. Greif, L. Gallmann, J. Osterwalder, M. Hengsberger, and U. Keller, Optica **2**, 405 (2015).
[3] Z. Tao, C. Chen, T. Szilvási, M. Keller, M. Mavrikakis, H. Kapteyn, and M. Murnane, Science **353**, 62 (2016).
[4] M. Schultze, M. Fiess, N. Karpowicz, J. Gagnon, M. Korbman, M. Hofstetter, S. Neppl, A. L. Cavalieri, Y. Komninos, T. Mercouris, C. A. Nicolaides, R. Pazourek, S. Nägele, J. Feist, J. Burgdörfer, A. M. Azzeer, R. Ernstorfer, R. Kienberger, U. Kleineberg, E. Goulielmakis, F. Krausz, and V. S. Yakovlev, Science **328**, 1658 (2010).
[5] K. Klünder, J. M. Dahlström, M. Gisselbrecht, T. Fordell, M. Swoboda, D. Guénot, P. Johnsson, J. Caillat, J. Mauritsson, A. Maquet, R. Taïeb, and A. L'Huillier, Phys. Rev. Lett. **106**, 143002 (2011).
[6] D. Guénot, K. Klünder, C. L. Arnold, D. Kroon, J. M. Dahlström, M. Miranda, T. Fordell, M. Gisselbrecht, P. Johnsson, J. Mauritsson, E. Lindroth, A. Maquet, R. Taïeb, A. L'Huillier, and A. S. Kheifets, Phys. Rev. A **85**, 053424 (2012).
[7] D. Guénot, D. Kroon, E. Balogh, E. W. Larsen, M. Kotur, M. Miranda, T. Fordell, P. Johnsson, J. Mauritsson, M. Gisselbrecht, K. Varjù, C. L. Arnold, T. Carette, A. S. Kheifets, E. Lindroth, A. L'Huillier, and J. M. Dahlström, J. Phys. B: At., Mol. Opt. Phys. **47**, 245602 (2014).
[8] E. P. Mansson, D. Guénot, C. L. Arnold, D. Kroon, S. Kasper, J. M. Dahlstrom, E. Lindroth, A. S. Kheifets, A. L'Huillier, S. L. Sorensen, and M. Gisselbrecht, Nat. Phys. **10**, 207 (2014).
[9] C. Palatchi, J. M. Dahlström, A. S. Kheifets, I. A. Ivanov, D. M. Canaday, P. Agostini, and L. F. DiMauro, J. Phys. B: At., Mol. Opt. Phys. **47**, 245003 (2014).
[10] M. Sabbar, S. Heuser, R. Boge, M. Lucchini, T. Carette, E. Lindroth, L. Gallmann, C. Cirelli, and U. Keller, Phys. Rev. Lett. **115**, 133001 (2015).
[11] M. Kotur, D. Guénot, A. Jimenez-Galan, D. Kroon, E. W. Larsen, M. Louisy, S. Bengtsson, M. Miranda, J. Mauritsson, C. L. Arnold, S. E. Canton, M. Gisselbrecht, T. Carette, J. M. Dahlstrom, E. Lindroth, A. Maquet, L. Argenti, F. Martin, and A. L'Huillier, Nat. Commun. **7**, 10566 (2016).
[12] A. S. Kheifets and I. A. Ivanov, Phys. Rev. Lett. **105**, 233002 (2010).
[13] J. M. Dahlström, A. L'Huillier, and A. Maquet, J. Phys. B: At., Mol. Opt. Phys. **45**, 183001 (2012).
[14] J. Dahlström, D. Guénot, K. Klünder, M. Gisselbrecht, J. Mauritsson, A. L'Huillier, A. Maquet, and R. Taieb, Chem. Phys. **414**, 53 (2013).
[15] A. S. Kheifets, Phys. Rev. A **87**, 063404 (2013).
[16] S. Neppl, R. Ernstorfer, E. M. Bothschafter, A. L. Cavalieri, D. Menzel, J. V. Barth, F. Krausz, R. Kienberger, and P. Feulner, Phys. Rev. Lett. **109**, 087401 (2012).
[17] S. Neppl, R. Ernstorfer, A. L. Cavalieri, C. Lemell, G. Wachter, E. Magerl, E. M. Bothschafter, M. Jobst, M. Hofstetter, U. Kleineberg, J. V. Barth, D. Menzel, J. Burgdorfer, P. Feulner, F. Krausz, and R. Kienberger, Nature **517**, 342 (2015).
[18] R. Pazourek, S. Nagele, and J. Burgdörfer, Rev. Mod. Phys. **87**, 765 (2015).
[19] H. J. Wörner, in Proceedings of the 3rd International Conference on "Correlation Effects in Radiation Fields," 13–18 September 2015.
[20] M. Huppert, I. Jordan, D. Baykusheva, A. von Conta, and H. J. Wörner, Phys. Rev. Lett. **117**, 093001 (2016).
[21] S. Kawai and A. D. Bandrauk, Phys. Rev. A **75**, 063402 (2007).
[22] J. C. Baggesen and L. B. Madsen, Phys. Rev. A **83**, 021403 (2011).
[23] I. A. Ivanov, A. S. Kheifets, and V. V. Serov, Phys. Rev. A **86**, 063422 (2012).
[24] X.-F. Hou, L.-Y. Peng, Q.-C. Ning, and Q. Gong, J. Phys. B: At., Mol. Opt. Phys. **45**, 074019 (2012).
[25] V. V. Serov, V. L. Derbov, and T. A. Sergeeva, Phys. Rev. A **87**, 063414 (2013).

[26]Q.-C. Ning, L.-Y. Peng, S.-N. Song, W.-C. Jiang, S. Nagele, R. Pazourek, J. Burgdörfer, and Q. Gong, Phys. Rev. A **90**, 013423 (2014).
[27]J. Caillat, A. Maquet, S. Haessler, B. Fabre, T. Ruchon, P. Salières, Y. Mairesse, and R. Taïeb, Phys. Rev. Lett. **106**, 093002 (2011).
[28]A. Chacon, M. Lein, and C. Ruiz, Phys. Rev. A **89**, 053427 (2014).
[29]P. Hockett, E. Frumker, D. M. Villeneuve, and P. B. Corkum, J. Phys. B: At., Mol. Opt. Phys. **49**, 095602 (2016).
[30]J. Cooper and R. N. Zare, J. Chem. Phys. **48**, 942 (1968).
[31]E. P. Wigner, Phys. Rev. **98**, 145 (1955).
[32]L. Eisenbud, "Formal properties of nuclear collisions," Ph.D. thesis, Princeton University, 1948.
[33]F. T. Smith, Phys. Rev. **118**, 349 (1960).
[34]A. P. Martin, Acta Phys. Austriaca **23**, 157 (1981).
[35]D. Boll, F. Gesztesy, and H. Grosse, J. Math. Phys. **24**, 1529 (1983).
[36]M. L. Goldberger and K. M. Watson, Phys. Rev. **127**, 2284 (1962).
[37]P. M. Paul, E. S. Toma, P. Breger, G. Mullot, F. Augé, P. Balcou, H. G. Muller, and P. Agostini, Science **292**, 1689 (2001).
[38]F. A. Gianturco, R. R. Lucchese, and N. Sanna, J. Chem. Phys. **100**, 6464 (1994).
[39]A. P. P. Natalense and R. R. Lucchese, J. Chem. Phys. **111**, 5344 (1999).
[40]R. R. Lucchese, K. Takatsuka, and V. McKoy, Phys. Rep. **131**, 147 (1986).
[41]R. R. Lucchese and D. Dowek, "Angular distributions in molecular photoionization," in *Attosecond and XUV Physics* (Wiley-VCH Verlag GmbH & Co. KGaA, 2014), pp. 293–320.
[42]H. Park and R. N. Zare, J. Chem. Phys. **104**, 4554 (1996).
[43]H. M. Nussenzveig, Phys. Rev. D **6**, 1534 (1972).
[44]In the case of collision scattering, the above equation needs to be modified to exclude the contribution at $\hat{k} \equiv (\theta_k, \phi_k) = (0, 0)$ that gives rise to an interference with the unscattered wave—a problem that does not arise in the context of photoionization.
[45]R. R. Lucchese, G. Raseev, and V. McKoy, Phys. Rev. A **25**, 2572 (1982).
[46]H. Stapelfeldt and T. Seideman, Rev. Mod. Phys. **75**, 543 (2003).
[47]P. M. Kraus, A. Rupenyan, and H. J. Wörner, Phys. Rev. Lett. **109**, 233903 (2012).
[48]P. M. Kraus, D. Baykusheva, and H. J. Wörner, Phys. Rev. Lett. **113**, 023001 (2014).
[49]P. M. Kraus, D. Baykusheva, and H. J. Wörner, J. Phys. B **47**, 124030 (2014).
[50]U. Fano, Phys. Rev. A **32**, 617 (1985).
[51]C. Brion and K. Tan, Chem. Phys. **34**, 141 (1978).
[52]C. M. Truesdale, S. Southworth, P. H. Kobrin, D. W. Lindle, and D. A. Shirley, J. Chem. Phys. **78**, 7117 (1983).
[53]T. A. Carlson, P. R. Keller, J. W. Taylor, T. Whitley, and F. A. Grimm, J. Chem. Phys. **79**, 97 (1983).
[54]E. Poliakoff, M.-H. Ho, M. White, and G. Leroi, Chem. Phys. Lett. **130**, 91 (1986).
[55]M. Braunstein and V. McKoy, J. Chem. Phys. **87**, 224 (1987).
[56]T. A. Ferrett, A. C. Parr, S. H. Southworth, J. E. Hardis, and J. L. Dehmer, J. Chem. Phys. **90**, 1551 (1989).
[57]L. A. Kelly, L. M. Duffy, B. Space, E. D. Poliakoff, P. Roy, S. H. Southworth, and M. G. White, J. Chem. Phys. **90**, 1544 (1989).
[58]R. T. Wiedmann, E. R. Grant, R. G. Tonkyn, and M. G. White, J. Chem. Phys. **95**, 746 (1991).